HCN IN BOK GLOBULES: A GOOD TRACER OF COLLAPSING CORES

José M. Afonso and João L. Yun

Departamento de Física, Universidade de Lisboa, Campo Grande, Edifício C1, 1700 Lisboa, Portugal; jafonso@astro.cc.fc.ul.pt, yun@astro.cc.fc.ul.pt

AND

Dan P. Clemens

Department of Astronomy, Boston University, 725 Commonwealth Avenue, Boston, MA 02215; clemens@protostar.bu.edu

ABSTRACT

We have conducted an HCN ($J = 1$–0) survey of dense cores in a sample of 24 star-forming and quiescent Bok globules. HCN emission was detected toward 11 of 13 globules containing embedded point sources, with no HCN detection among 11 starless globules. As in other dark clouds, the $J = 1$–0 hyperfine line intensity ratios vary from globule to globule and also with position toward the same globule, suggesting the presence of either a scattering envelope surrounding the core or a complex density structure. We find that the $J = 1$–0 transition of the HCN molecule can be used effectively to search for early stages of star formation in small molecular clouds: in the sample of star-forming cores, for three (of five) sources mapped, there is good spatial coincidence (better than 6″) between the position of the peak integrated HCN emission and the location of the associated embedded source. Furthermore, this transition is well correlated with the young stellar object (YSO) class, detecting preferentially class I YSOs. Our results indicate that detecting strong (>1 K km s^{-1}) HCN emission from a molecular cloud core seems to imply the presence of an embedded protostar and thus, indirectly, that of a collapsing core.

Key words: ISM: globules — ISM: molecules

1. INTRODUCTION

Star formation occurs in the densest regions of the molecular component of the interstellar medium. Both giant molecular clouds and dark clouds contain smaller and denser regions, the dense cores, whose collapse leads ultimately to the formation of a single star or a group of stars. However, many of the details of this process are still unknown. In particular, we would like to understand better the physical conditions existing just prior to the onset of core collapse, or the evolution from a dense core to the first appearance of a young pointlike stellar source.

Molecular hydrogen gas can be traced with observations of other molecular transitions. While the CO molecule is often used to trace H_2, the low dipole moment of CO (0.1 D) implies that the lower rotational CO transitions do not trace dense gas: instead, they delineate the extent of the molecular cloud. Molecules with higher dipole moments are needed to search for dense cores within a cloud. For example, the $J = 1$–0 transition of the HCN molecule (dipole moment of 3 D) traces gas with densities $n \gtrsim 10^4$–10^5 cm^{-3} (see, e.g., Turner 1974), i.e., about 100 times denser than traced by the corresponding CO transition.

In order to study the physical properties of the dense cores and their relationships to the formation of the young stellar objects (YSOs) found embedded in the cores, we have conducted a HCN survey, using the $J = 1$–0 line transition, in a sample of 24 Bok globules.

Bok globules, the simplest and least massive dark molecular clouds known in the Galaxy, are nearby, fairly isolated, and usually display regular shapes (Clemens & Barvainis 1988). As such, they are constrained to be the sites of mostly low-mass star formation. They offer a uniquely clean laboratory for studying star formation and probing the physical properties present in molecular clouds and cores prior to the onset of gravitational collapse.

Low-mass star formation is a rather common phenomenon in Bok globules (see, e.g., Yun & Clemens 1990, 1994a; Alves & Yun 1995; Moreira & Yun 1995). Detecting star formation in a globule often starts with a detection of an infrared, centimeter, or (sub-) millimeter source toward the globule, followed by a proof of its association with the globule (Yun & Clemens 1994a, 1994b; Yun et al. 1996; Launhardt, Ward-Thompson, & Henning 1997). In this work, we have used the *IRAS* database and previous studies of Bok globules (Yun & Clemens 1994a, 1994b) to correlate HCN detections with the presence and location of globule-associated point sources.

By searching for HCN emission from a sample of clouds containing quiescent and star-forming examples (i.e., containing starless globules and globules with YSOs in different evolutionary stages), we are probing the physical conditions of the different evolutionary stages of a small molecular cloud during the star formation process. In particular, we are able to estimate the duration of detectable HCN emission and we link this emission with the presence of protostellar sources embedded in the globules.

In this paper, we present the results of our HCN survey of dense cores in Bok globules. Applications of these results to studies of the star formation process ocurring in small molecular clouds are discussed. In § 2 we describe the observations and data reduction, in § 3 we present and discuss our results, and in § 4 we summarize our conclusions.

2. OBSERVATIONS AND DATA REDUCTION

Millimeter observations at 88.63 GHz ($J = 1$–0 rotational transition of HCN) were carried out toward a sample of 24 Bok globules (Table 1) using the 15 m Swedish-ESO Submillimetre Telescope of the European Southern Observatory during 1994 March 16–23. The half-power beam-

TABLE 1

HCN SURVEY OF DENSE CORES IN BOK GLOBULES

Bok Globule (1)	R.A. (B1950) (2)	Decl. (B1950) (3)	Associated Point Source (4)	V_{LSR} (km s^{-1}) (5)	Δv_{FWHM} (km s^{-1}) (6)	$T_R^{F=2-1}$ (K) (7)	$I_{HCN}^{F=2-1}$ (K km s^{-1}) (8)	T_R (K) (9)	I_{HCN} (K km s^{-1}) (10)
CB 29	05 19 28.0	−03 43 26	...	...	...	<0.16	<0.22	<0.16	<0.22
CB 31/LBN 913	05 30 45.2	−00 38 15	II	−7.1	0.5 (0.1)	0.55 (0.07)	0.24 (0.04)	0.55 (0.07)	0.24 (0.04)
CB 32/LBN 921	05 33 47.5	−00 19 05	II	−5.1	0.3 (0.1)	0.67 (0.08)	0.19 (0.02)	0.67 (0.08)	0.19 (0.02)
CB 33	05 43 38.0	20 44 26	...	...	...	<0.13	<0.18	<0.13	<0.18
CB 34[a,b]	05 44 02.8	20 59 07	I	0.6	2.2 (0.1)	0.77 (0.07)	1.60 (0.07)	1.56 (0.21)	3.48 (0.18)
CB 39	05 59 06.0	16 30 58	II	2.4	0.5 (0.1)	0.67 (0.08)	0.30 (0.04)	0.67 (0.08)	0.30 (0.04)
CB 47	06 17 15.0	07 09 33	...	...	...	<0.19	<0.26	<0.19	<0.26
CB 50	06 31 36.3	07 48 10	II	...	...	<0.11	<0.15	<0.11	<0.15
CB 52	06 46 25.3	−16 50 38	II	...	...	<0.19	<0.26	<0.19	<0.26
CB 54/LBN 1042[a]	07 02 06.0	−16 18 47	I	19.6	2.9 (0.1)	0.69 (0.03)	2.01 (0.03)	1.57 (0.09)	4.05 (0.08)
CB 57	07 15 27.0	−22 56 07	...	...	...	<0.10	<0.14	<0.10	<0.14
CB 58[a]	07 16 09.1	−23 36 11	I	15.1	1.6 (0.1)	0.29 (0.04)	0.47 (0.03)	0.65 (0.12)	0.99 (0.08)
CB 60/L1670	08 02 38.2	−31 22 09	II	14.2	1.3 (0.3)	0.24 (0.08)	0.21 (0.05)	0.24 (0.08)	0.21 (0.05)
CB 68[a]	16 54 27.2	−16 04 48	I	5.3	0.9 (0.1)	1.29 (0.09)	1.01 (0.06)	2.92 (0.27)	2.24 (0.16)
CB 69/B49	16 59 31.1	−33 11 15	...	...	...	<0.11	<0.15	<0.11	<0.15
CB 75/B247	17 09 56.3	−30 12 22	...	...	...	<0.12	<0.17	<0.12	<0.17
CB 77	17 12 39.0	−01 40 00	...	...	...	<0.09	<0.12	<0.09	<0.12
CB 81/L1774	17 19 22.9	−27 05 56	...	...	...	<0.09	<0.12	<0.09	<0.12
CB 103	17 52 48.0	−02 48 19	...	...	...	<0.12	<0.17	<0.12	<0.17
CB 108/L262[a]	18 00 07.1	−20 53 07	II	5.7	1.5 (0.1)	0.41 (0.05)	0.67 (0.04)	0.93 (0.15)	1.21 (0.11)
CB 145/L443	18 29 21.9	−09 12 16	...	...	...	<0.12	<0.17	<0.12	<0.17
CB 155/B104	18 44 41.5	−04 35 14	...	...	...	<0.19	<0.26	<0.19	<0.26
CB 188	19 17 54.0	11 29 56	I	7.1	1.3 (0.2)	0.19 (0.04)	0.22 (0.03)	0.33 (0.08)	0.34 (0.06)
CB 205/L810	19 43 21.7	27 43 37	I	15.9	1.9 (0.1)	1.33 (0.07)	2.60 (0.05)	2.60 (0.21)	4.69 (0.15)

NOTES.—Errors are 1 σ and upper limits are 2 σ. Units of right ascension are hours, minutes, and seconds, and units of declination are degrees, arcminutes, and arcseconds.

[a] Mapped in a grid of positions. Cols. (2) and (3) indicate the coordinates of the center of the map.

[b] Cols. (5)–(10) refer to a position with an offset of $(\Delta R.A., \Delta decl.) = (0\rlap{.}''767, 0')$.

width of the telescope was 56″ at the observed frequency, with a main-beam efficiency of 0.75. The back end included a 1000-channel acousto-optical spectrometer with 43 kHz resolution (0.15 km s^{-1}). Each Bok globule was observed using dual beam switching (chop throw of 11′), with integration times between 10 and 20 minutes on each position. The pointing error was found to be better than 6″. Spectral line intensities were calibrated and corrected for atmospheric losses using the standard chopper-wheel method to obtain the antenna temperature T_A^*. The data were processed using standard procedures of the Continuum and Line Analysis Single-dish Software (CLASS) package developed at the Observatoire de Grenoble and IRAM Institute. Baselines were fitted and removed, followed by Gaussian fitting, yielding the values of the line parameters (peak, width, and integrated intensity). Detection limits (2 σ) are given in Table 1 and range from 0.04 to 0.26 K km s^{-1}, with most values around 0.10 K km s^{-1}.

3. RESULTS AND DISCUSSION

In Table 1, we list the globules observed. Columns (2) and (3) give the positions observed toward each globule or the coordinates of the center of the maps (when observed in more than one position). Column (4) indicates whether a YSO is associated with the globule and the YSO class (Yun & Clemens 1995), according to the classification of Adams, Lada, & Shu (1987) extended by André, Ward-Thompson, & Barsony (1993). When an *IRAS* Point Source Catalog (PSC) source is associated with a globule (as indicated in col. [4]), the positions listed in columns (2) and (3) are those of the *IRAS* PSC sources. In the remaining cases, columns (2) and (3) list the positions of the optical center of the globule (Clemens & Barvainis 1988). Columns (5)–(10) give

the results of the HCN survey. Columns (5), (6), (7), and (8) list respectively the line velocity V_{LSR}, the FWHM line width Δv, the line peak T_R (antenna temperature corrected for the main-beam efficiency), and the integrated line intensity (area, $I_{HCN} = \int T_R\, dv$) for the central line component ($F = 2-1$ transition, usually the most intense). Columns (9) and (10) give respectively the line peak and the integrated line intensity of the three hyperfine components summed together. Values in parentheses are 1 σ errors, and upper limits are 2 σ. For nondetections, the upper limit in the integrated emission, σ_I, is the area of a Gaussian line with peak intensity equal to σ_{T_R} and FWHM equal to the largest Δv_{FWHM} among the weakest detections.

3.1. *Spectra and Maps*

The $J = 1-0$ rotational transition of the HCN molecule exhibits a hyperfine structure (due mainly to the nuclear quadrupole moment of the nitrogen atom). The main line splits into three components: $F = 0-1$ (88633.9 MHz), $F = 2-1$ (88631.8 MHz), and $F = 1-1$ (88630.4 MHz) (see, e.g., De Lucia & Gordi 1969; Bogey, Demuynck, & Destombes 1981). The theoretical values for the relative intensities of these three components are approximately 1 : 5 : 3 (see, e.g., González-Alfonso & Cernicharo 1993). These components represent the spectral signature of the HCN $J = 1-0$ transition and allow a simple identification of the HCN detection. As an example, Figure 1 shows spectra obtained toward CB 68 and CB 54.

Whenever the line seen was strong, additional spectra were taken in an approximately full-beam spacing grid. An example is shown in Figure 2, where the spectra of CB 68 are shown. The horizontal velocity axis and the vertical antenna temperature axis are the same as in Figure 1.
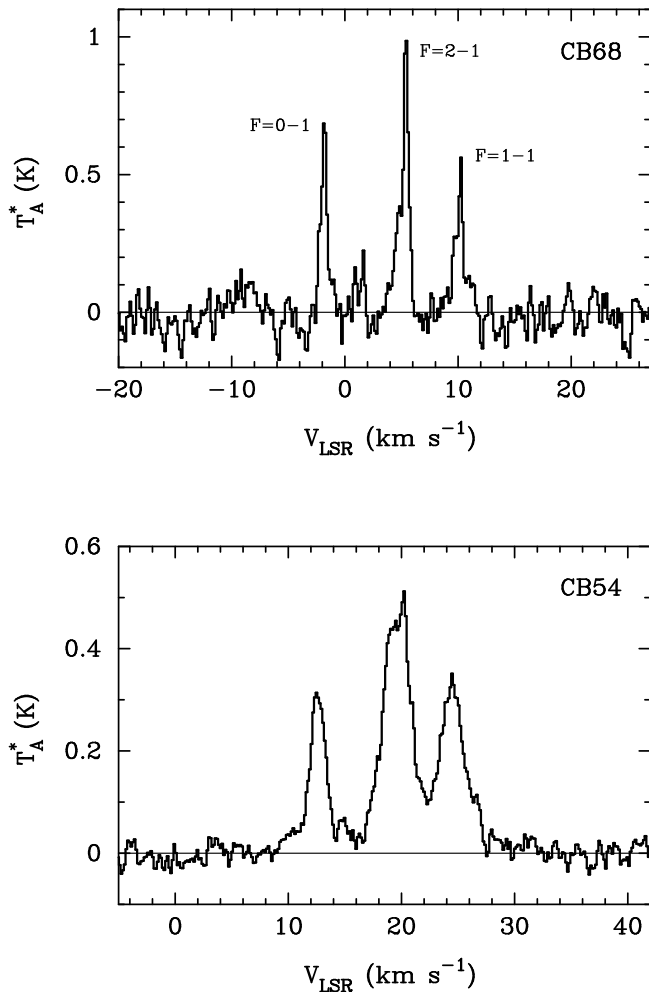
FIG. 1.—Example of spectra obtained toward CB 68 and CB 54. The hyperfine splitting of the $J = 1$–0 rotational line of HCN is clearly seen. Note that the ratio between the intensities of the different components is not the same in the two globules, and does not coincide with the theoretical value of 1:5:3.

From the HCN spectra in Figures 1 and 2, we verify that the relative intensities do not match the theoretical values and vary from cloud to cloud, as well as within the same cloud. This has been found in previous observations of HCN in dark clouds (Walmsley et al. 1982; Sandell, Höglund, & Kislyakov 1983; Cernicharo et al. 1984). In most cases, the $F = 2$–1 (88631.8 MHz) and $F = 1$–1 (88630.4 MHz) lines keep close to their theoretical ratio, while the optically thinnest $F = 0$–1 (88633.9 MHz) line appears more intense than it should. This effect has been suggested (Cernicharo et al. 1984) to be due to scattering in an envelope surrounding the cloud core. In other cases, toward very high density regions, such as the densest regions of Heiles's cloud 2 or of TMC-1 (Walmsley et al. 1982), the optically thinnest $F = 0$–1 line is strongly enhanced, becoming the strongest of the three components. This behavior is seen also in Figure 2, where the ratio of the intensities of the $F = 0$–1 line (the left of the three components) and the $F = 2$–1 line (central) varies rapidly across the cloud core, reaching values in excess of 1 at some positions.

In Figure 3, we present the contour maps for those globules where the line was detected at different positions in the grid (the emission was resolved). At the resolution of our observations, the maps in Figure 3 reveal regular shapes. Based on these maps, an estimate of the angular size of the emitting region could be made. This represents the angular size of the dense cores in these Bok globules. The FWHM angular diameters obtained were 1′.7, 1′.3, 1′.3, 1′.6, and 1′.4, respectively, for CB 34, CB 54, CB 58, CB 68, and CB 108. For an average distance of about 600 pc (Clemens & Barvainis 1988), these values correspond to diameters of the order of 0.3 pc.

For CB 54, CB 58, and CB 68, there is good spatial coincidence between the peaks of their HCN emissions and the associated *IRAS* PSC sources located at the origin. This spatial coincidence is poorer for CB 34, where an offset of about 1′ exists. However, at the position of the *IRAS* PSC source the HCN emission is also strong. This offset agrees with the conclusions of Alves & Yun (1995) and of Moreira & Yun (1995), whose optical and near-infrared images suggested the presence of a dense core located northeast of the *IRAS* source. CB 34 has been shown (Alves & Yun 1995) to have formed a small aggregate of YSOs, with possible sequential star formation proceeding roughly from southwest to northeast. The dense HCN core revealed in Figure 3*a* may be the next star formation site within CB 34 (i.e., the location where new young stellar sources are currently starting to form). Finally, the larger offset seen in the map of CB 108 (Fig. 3*e*) is the exception to this general good agreement between HCN peak emission and embedded *IRAS* sources. In this case, however, the YSO is a class II source, and contamination or confusion caused by crowding seen toward the Galactic center region may prevent a reliable association.

3.2. Optical Depths

$H^{13}CN$ $J = 1$–0 spectra were obtained toward the strongest sources. We could find $H^{13}CN$ emission just in one case, that of CB 54, with a T_R of 0.14 ± 0.03 K, for the $F = 2$–1 line. Assuming a solar isotopic ratio $^{12}C/^{13}C$ of 89, we have determined the optical depths τ_{13} and τ_{12} at the central position of CB 54. The values obtained were, respectively, 0.16 and 12.65, indicating that the $H^{13}CN$ emission is optically thin, while HCN is generally optically thick.

3.3. HCN, Starless Globules, and Class I sources

Analysis of Table 1 indicates that there is a correlation between the strength of the HCN detection in a globule and the presence of an associated class I source. In order to better investigate this correlation, we have plotted, in Figure 4, the integrated line intensity of the three hyperfine components given in column (10) of Table 1 versus the class of the associated YSO. Each circle and horizontal line in Figure 4 corresponds to one globule and its associated YSO. The globules without an associated embedded source appear in the class of "starless" globules. Arrows represent upper limits. We have included in this figure additional Bok globule HCN data from other authors: CB 6/LBN 613, CB 216/L797, CB 244/L1262 (Scappini et al. 1994), and CB 199/B335 (Harju 1989). From left to right and from top to bottom, the globules represented in this figure are as follows:

Starless.—CB 47, CB 155/B104, CB 33, CB 75/B247, CB 103, CB 145/L443, CB 69/B49, CB 57, CB 77, CB 81/L1774, CB 29;
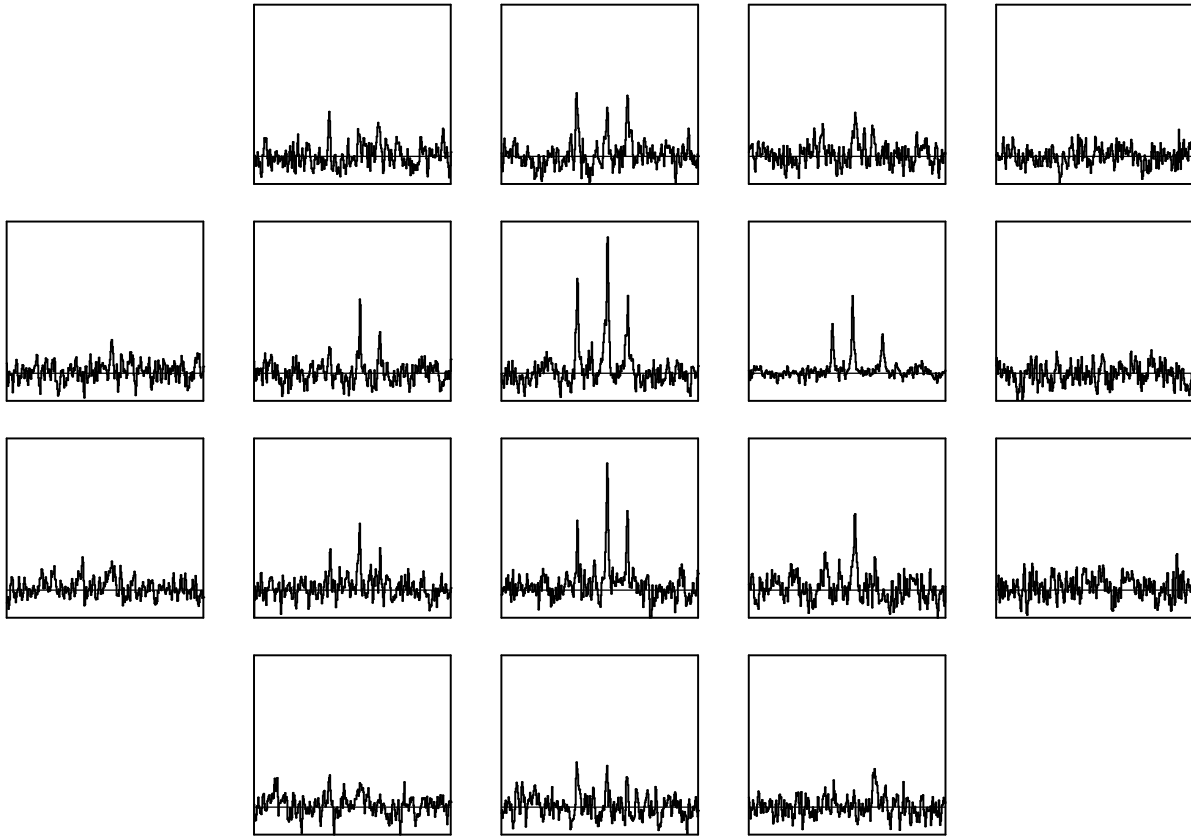
Class 0.—CB 199/B335;

FIG. 2.—Map of HCN emission line profiles for CB 68. The spectra are presented in their relative angular positions. The horizontal velocity axis and the vertical antenna temperature axis are the same as in Fig. 1.

Class I.—CB 205/L810, CB 54/LBN 1042, CB 34, CB 244/L1262, CB 68, CB 58, CB 6/LBN 613, CB 216/L797, CB 188;

Class II.—CB 108/L262, CB 52, CB 39, CB 50, CB 31/LBN 913, CB 60/L1670, CB 32/LBN 921.

Figure 4 shows that no HCN detection occurred for starless globules. In addition, strong HCN emission was detected only toward the globules with associated class I sources. This group of globules appears as a distinct group when we consider the presence of strong HCN emission (defined here as $I_{HCN} > 1$ K km s^{-1}). In this group of globules, more than half exhibit strong HCN emission, while only one globule without an associated class I source reaches strong HCN emission. This is clearly seen in Figure 5. This figure shows the cumulative fraction of sources with integrated intensities smaller than or equal to a fixed value. The line to the right corresponds to the group of globules with an associated class I source; the line to the left corresponds to the group without an associated class I source. About 65% of the sources in the former group have strong HCN emission, whereas this is true for only 5% of sources in the latter group. The probability that the values of I_{HCN} observed for the two data sets (class I group and non–class I group) come from a single parent distribution is 0.01% (Kolmogorov-Smirnov test).

The absence of HCN emission in the group of starless globules seems to indicate that the stage of the star formation process between the instant when the cloud core becomes sufficiently dense to excite the HCN $J = 1-0$ transition and the appearance of a point source is very brief. If

the horizontal axis in Figure 4 is seen as a temporal axis, the concentration of strong detections seen in this figure indicates that HCN emission is a relatively transient phenomenon, and that strong emission occurs only during the period of the protostellar accretion. This is in good agreement with estimates of the timescales for the formation of a dense core and for protostellar accretion, as is described in the following paragraph.

Low-mass stars typically form within cold, dense, weakly magnetized, and magnetically subcritical cloud cores (see, e.g., Myers & Benson 1983). These clouds undergo a quasi-static contraction as a result of ambipolar diffusion that leads to a slow increase of the central density and mass-to-flux ratio. This ambipolar diffusion period, lasting for about 15 Myr (Fiedler & Mouschovias 1993), ends when the ratio of mass to magnetic flux reaches a value where the cloud core ceases to be subcritical, allowing the gravitational collapse to finally occur. The timescale for the subsequent gravitational collapse and protostellar accretion stage is typically 0.1–1 Myr (Shu 1977; Stahler, Shu, & Taam 1980). At the end of this stage, the dense core contains a point source. From these numbers, we can see that the accretion timescale is much smaller than the ambipolar diffusion timescale. Furthermore, interestingly, according to the theoretical models of Fiedler & Mouschovias (1993), the value of the central density in a cloud core corresponding to the end of the ambipolar diffusion stage (and the start of the accretion stage) roughly coincides with that required to excite the HCN $J = 1-0$ transition ($\sim 10^4-10^5$ cm^{-3}). Together, these facts could explain the absence of strong HCN core emitters without an associated point source. It
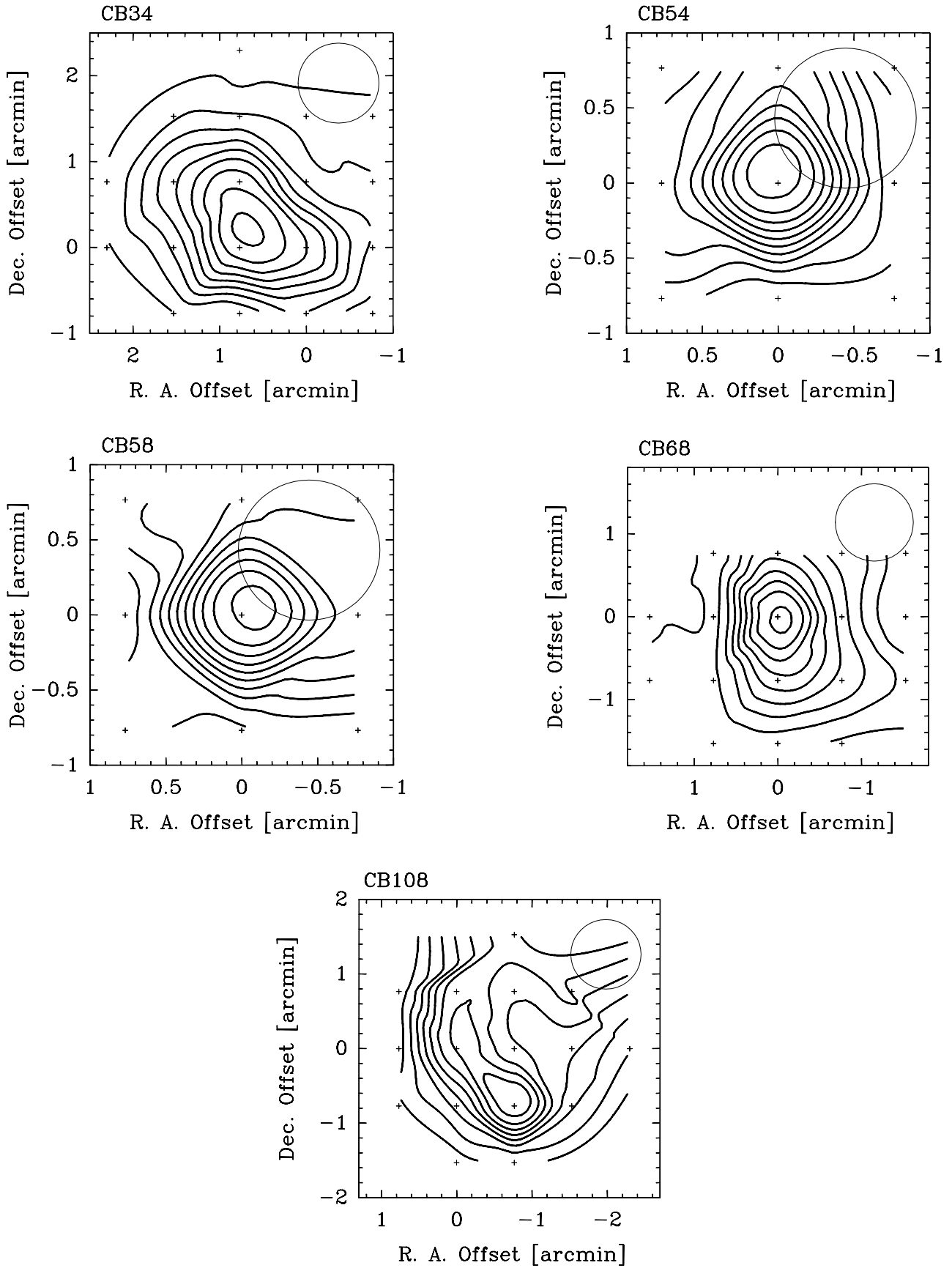
Fig. 3.—Contour plots of the HCN line integrated emission for five globules with resolved emission. (*a*) CB 34; contours begin at 0.4 K km s^{-1} and are stepped by 0.4 K km s^{-1}. (*b*) CB 54; contours begin at 1.2 K km s^{-1} and are stepped by 0.3 K km s^{-1}. (*c*) CB 58; contours begin at 0.25 K km s^{-1} and are stepped by 0.08 K km s^{-1}. (*d*) CB 68; contours begin at 0.6 K km s^{-1} and are stepped by 0.2 K km s^{-1}. (*e*) CB 108; contours begin at 0.30 K km s^{-1} and are stepped by 0.15 K km s^{-1}. The associated *IRAS* PSC source is located at the center of the maps. Circles show HCN FWHM beam sizes.
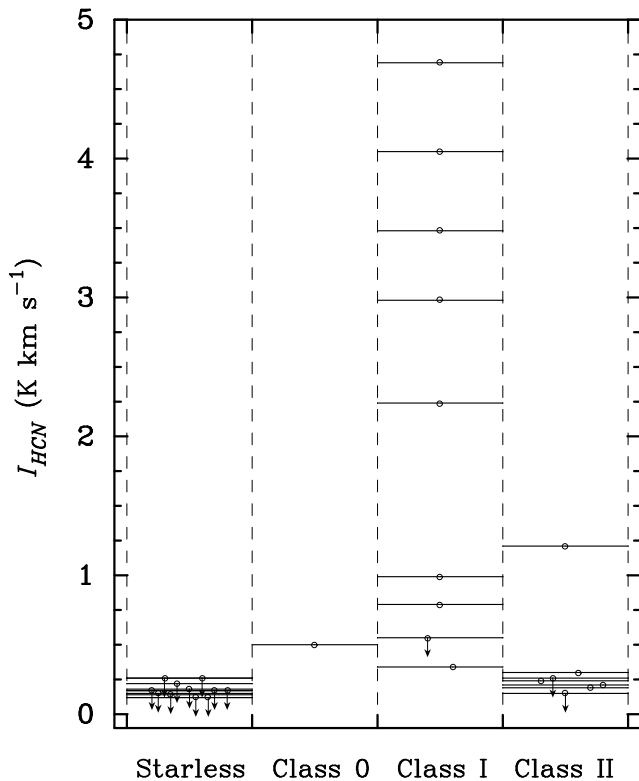
FIG. 4.—HCN emission and the presence (or absence) of a point source. No HCN emission was detected toward a starless globule. All strong emissions were detected toward globules with an associated class I source. See § 3.3 for a description.
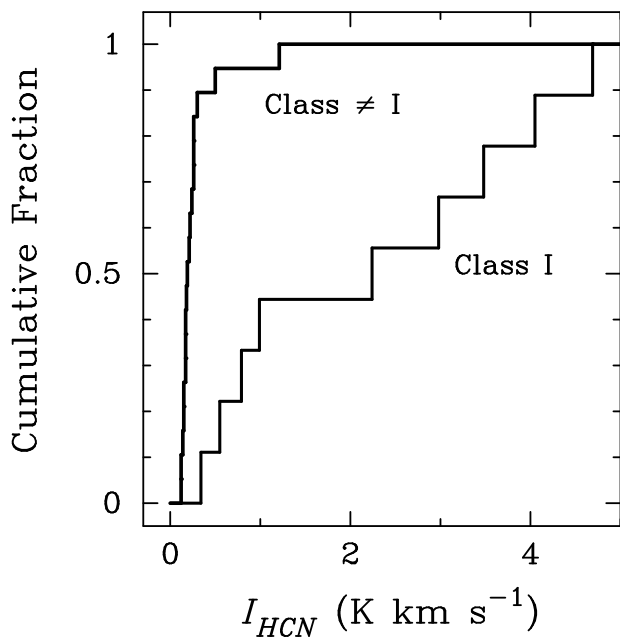

FIG. 5.—Cumulative fraction of globules with HCN integrated intensity smaller or equal to a fixed value. The line to the right refers to the globules with associated class I sources; the line to the left refers to the starless globules or those with non–class I sources. Note the large number of sources with large I_{HCN} values in the class I group sources. Sixty percent of the class I group sources have $I_{HCN} > 1$ K km s^{-1}, while this is the case for only 10% of the non–class I group sources.

appears that once a cloud core reaches a sufficiently high density, enabling HCN excitation and the start of protostellar accretion, it will rapidly form a YSO (first detected as a class I or class 0 source). As a result, we expect that it should be very difficult to detect a core with strong HCN emission and no YSO.

In this argument, we have not distinguished between class I and class 0 sources. We expect that class 0 sources should also be relatively strong HCN emitters. The small number (just one globule, from the literature) of class 0 sources in our sample does not allow us to test that hypothesis. Future observations of HCN in this class of sources should be able to answer this question.

On the other hand, cloud dispersal, caused by the powerful stellar jets and outflows, leads the evolving YSO into its class II phase and is probably responsible for the disappearance of the HCN emission among class II sources (Fig. 4). Alternatively, the lack of HCN emission from class II objects may be due to depletion of HCN onto grains at the densities of the circumstellar disks surrounding those objects (see, e.g., Bergin, Langer, & Goldsmith 1995; Langer, Velusamy, & Xie 1996).

Finally, we note that our findings tend to point to a clear distinction between the use of ammonia and of HCN in tracing dense cores. Since the work of Myers & Benson (1983), ammonia has been used to identify dense cores in dark clouds. Myers et al. (1987) have found that about half of the ammonia dense cores were associated with *IRAS* sources, while the other half were starless. Lemme et al. (1996), in their survey of ammonia in Bok globules, have found a large number of starless globules exhibiting strong NH$_3$ (1,1) emission. The fraction of starless globules among strong ammonia detections is 58% (and this number increases if we consider all globules), a very different result from our 0% of starless HCN cores. We thus conclude that while ammonia traces dense cores, HCN is more selective, detecting cores with embedded (class 0, class I, or class II) objects, and thus indirectly tracing the presence of collapsing cores. In particular, strong (>1 K km s^{-1}) HCN emission is a useful tool for locating class I objects.

4. SUMMARY

1. We have conducted HCN ($J = 1$–0) observations of a sample of 24 Bok globules. Of the 24 sources, 11 were starless (with no evidence for embedded sources), six were associated with class I sources, and seven were associated with class II sources.

2. HCN emission was detected toward 11 clouds (six class I and five class II sources), with no HCN detection among the starless globules.

3. Strong (>1 K km s^{-1}) HCN emission from a globule core is found to be very well correlated with the presence of an embedded class I source.

4. When the globule HCN emission is resolved, we verify that the spatial distribution of the HCN emission tends to peak at the position of the associated point source.

5. As in other dark clouds, the intensities of the hyperfine components do not coincide with the theoretical values, and vary from globule to globule and within the same globule, suggesting the presence of a scattering envelope surrounding the dense core.

6. The physical conditions required to excite strong HCN ($J = 1$–0) emission are reached when a protostellar core has formed.

5. CONCLUSIONS

1. The strong presence of the $J = 1-0$ transition of the HCN molecule signifies recent star formation in small molecular clouds. Detecting strong (> 1 K km s^{-1}) HCN emission seems to imply the presence of a collapsing core.

2. The $J = 1-0$ transition of the HCN molecule preferentially detects class I YSOs.

3. There appears to be no time delay between when HCN ($J = 1-0$) becomes detectable and when a point source is found.

4. The physical conditions required to excite strong HCN $J = 1-0$ emission are reached at about the end of the ambipolar diffusion stage or the beginning of the protostellar accretion stage in a small molecular cloud.

REFERENCES

Adams, F. C., Lada, C. J., & Shu, F. H. 1987, ApJ, 312, 788
Alves, J. F., & Yun, J. L. 1995, ApJ, 438, L107
André, P., Ward-Thompson, D., & Barsony, M. 1993, ApJ, 406, 122
Bergin, E. A., Langer, W. D., & Goldsmith, P. F. 1995, ApJ, 441, 222
Bogey, M., Demuynck, C., & Destombes, J. L. 1981, Molec. Phys., 43, 1043
Cernicharo, J., Castets, A., Duvert, G., & Guilloteau, S. R. 1984, A&A, 139, L13
Clemens, D. P., & Barvainis, R. 1988, ApJS, 68, 257
De Lucia, F., & Gordi, W. 1969, Phys. Rev., 187, 58
Fiedler, R. A., & Mouschovias, T. C. 1993, ApJ, 415, 680
González-Alfonso, E., & Cernicharo, J. 1993, A&A, 279, 506
Harju, J. 1989, A&A, 219, 293
Moreira, M. C., & Yun, J. L. 1995, ApJ, 454, 850
Langer, W. D., Velusamy, T., & Xie, T. 1996, ApJ, 468, L41
Launhardt, R., Ward-Thompson, D., & Henning, T. 1997, MNRAS, 288, 45
Lemme, C., Wilson, T. L., Tieftrunk, A. R., & Henkel, C. 1996, A&A, 312, 585

Myers, P. C., & Benson, P. J. 1983, ApJ, 266, 309
Myers, P. C., Fuller, G. A., Mathieu, R. D., Beichman, C. A., Benson, P. J., Schild, R. E., & Emerson, J. P. 1987, ApJ, 319, 340
Sandell, G., Höglund, B., & Kislyakov, A. G. 1983, A&A, 118, 306
Scappini, F., Palumbo, G. G. C., Bruni, G., & Bergman, P. 1994, ApJ, 427, 259
Shu, F. H. 1977, ApJ, 214, 488
Stahler, S. W., Shu, F. H., & Taam, R. E. 1980, ApJ, 241, 637
Turner, B. E. 1974, in Galactic and Extra-galactic Radio Astronomy, ed. G. L. Verschuur & K. I. Kellermann (New York: Springer), 199
Walmsley, C. M., Churchwell, E., Nash, A., Fitzpatrick, E. 1982, ApJ, 258, L75
Yun, J. L., & Clemens, D. P. 1990, ApJ, 365, L73
———. 1994a, AJ, 108, 612
———. 1994b, ApJS, 92, 145
———. 1995, AJ, 109, 742
Yun, J. L., Moreira, M. C., Torrelles, J. M., Afonso, J. M., & Santos, N. C. 1996, AJ, 111, 841